

Stroboscopic observation of quantum many-body dynamics

Stefan Keßler,¹ Andreas Holzner,² Ian P. McCulloch,³ Jan von Delft,² and Florian Marquardt^{1,4}

¹*Institute for Theoretical Physics, Universität Erlangen-Nürnberg, Staudtstr. 7, DE-91058 Erlangen, Germany*

²*Physics Department, Arnold Sommerfeld Center for Theoretical Physics, and Center for NanoScience, Ludwig-Maximilians-Universität München, Theresienstr. 37, DE-80333 München, Germany*

³*School of Physical Sciences, The University of Queensland, Brisbane, Queensland 4072, Australia*

⁴*Max Planck Institute for the Science of Light, Günther-Scharowsky-Straße 1/Bau 24, DE-91058 Erlangen, Germany*

Recent experiments have demonstrated single-site resolved observation of cold atoms in optical lattices. Thus, in the future it may be possible to take repeated snapshots of an interacting quantum many-body system during the course of its evolution. Here we address the impact of the resulting quantum (anti-)Zeno physics on the many-body dynamics. We use the time-dependent density-matrix renormalization group to obtain the time evolution of the full wave function, which is then periodically projected in order to simulate realizations of stroboscopic measurements. For the example of a one-dimensional lattice of spinless fermions with nearest-neighbor interactions, we find regimes for which many-particle configurations are stabilized or destabilized, depending on the interaction strength and the time between observations.

PACS numbers: 67.85.-d, 03.65.Xp, 71.10.Fd

Introduction. In the last few years ultracold atoms in optical lattices have proven to be a versatile tool for studying various quantum many-body phenomena [1, 2]. Recently, tremendous progress has been achieved by implementing single-site resolved detection [3, 4] and addressing [5] of atoms. Taken to the next, dynamic level, one may envision observing the evolution of nonequilibrium quantum many-body states via periodic snapshots revealing the position of each single atom. For simpler systems, the effect of frequent observations on the decay of an unstable state (or on the dynamics of a driven transition) has already been discussed and observed, leading to the notion of the quantum (anti-)Zeno effect [6–9]. Zeno physics has also been seen in cold-atom experiments with atomic loss channels [10] and was theoretically addressed in [11–14]. Experiments with single-site detection, however, would reveal the effect of observations on the dynamics of a truly interacting quantum many-body system. Here we exploit a numerically efficient approach to simulating the repeated observation of many-particle configurations in interacting lattice models. This represents an idealized version of the dynamics that may be realized in future experiments. We elaborate the main features of this “stroboscopic” many-body dynamics in the case of a one-dimensional (1D) lattice of spin-polarized fermions with nearest-neighbor interactions. We find a variant of the quantum Zeno effect and discuss its tendency to inhibit or accelerate the breakup of certain many-particle configurations. In particular, the decay rate of these configurations depends in a *nonmonotonous* fashion on the time interval between observations. Later, we show that a similar behavior is expected for the Fermi-Hubbard and Bose-Hubbard model. The discussed features may be seen, e. g., in the expansion of interacting atomic clouds in a lattice.

Model. In this paper, we study spin-polarized fermions

in a 1D lattice governed by the Hamiltonian

$$\hat{H} = -J \sum_i (\hat{c}_i^\dagger \hat{c}_{i+1} + \text{H.c.}) + V \sum_i \hat{n}_i \hat{n}_{i+1}. \quad (1)$$

The first term describes hopping with amplitude J between adjacent sites, the second encodes the interaction between fermions at neighboring sites, with $\hat{n}_i = \hat{c}_i^\dagger \hat{c}_i$. The Hamiltonian displays a dynamical $V \mapsto -V$ symmetry which shows up in expansion experiments [15]. Following analogous steps as in [15], we can conclude that if both the initial state and the experimentally measured quantity \hat{O} are invariant under both time reversal and π -boost (a translation of all momenta by π), the observed time evolution $\langle \hat{O}(t) \rangle$ is identical for repulsive and attractive interactions of the same strength. The initial occupation number states and the n -particle density observables in our case fall within the scope of this theorem. Thus, the only relevant dimensionless parameters are $|V/J|$ and the rescaled time between observations, $J\Delta t$.

Single particle. We first briefly turn to the single-particle case, in which Eq. (1) leads to a tight-binding band $E(k) = -2J \cos(k)$. A particle located initially at a single site is in a superposition of all plane wave momenta $k = -\pi \dots \pi$. After a time t , the probability of detecting it at a distance l from the initial site is $\rho(l, t) = \mathcal{J}_{|l|}^2(2Jt)$, where \mathcal{J} is the Bessel function of the first kind. This is shown in Fig. 1(a). The particle moves ballistically, with $\langle l^2 \rangle = 2(Jt)^2$. When the particle is observed repeatedly, at intervals Δt , the ballistic motion turns into diffusion. In this case, after m time steps of duration $\Delta t = t/m$, we have $\langle l^2 \rangle = 2J^2 t \Delta t$. Thus the motion slows down, and in the limit of an infinite observation rate, the particle is frozen, which is known as the quantum Zeno effect.

Simulation. Ideally, each observation is a projective measurement in the basis of many-particle configurations

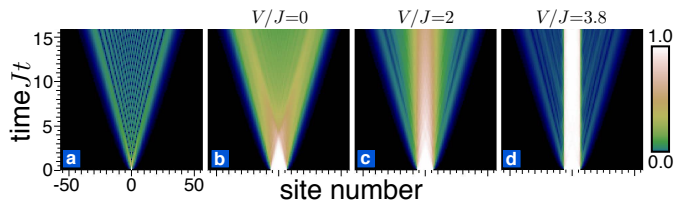


Fig. 1. (Color online) Time evolution of the density profile of fermions expanding in a lattice without observation, (a) for a single fermion; (b)-(d) for 13 fermions, initially located at adjacent lattice sites, calculated for several interaction strengths.

(occupation number states in real space). To generate such measurement outcomes in a numerically efficient way, we start by randomly drawing the position of the first particle from a distribution given by the one-particle density. Afterward, we draw the position of the second particle, *conditioned* on the location of the first one, and proceed iteratively (see Supplemental Material [16] for details). For the interacting many-body case to be discussed now, we use the time-dependent density-matrix renormalization group (tDMRG) [17–20] to calculate the joint probabilities and the time evolution between observations. We choose a time step of $J\delta t = 0.1$ and a lattice of typically 115 sites, and we keep up to approximately 1000 states, at a truncation error of 10^{-6} . For the dynamics of noninteracting fermions, an exact formula can be used (see Supplemental Material [16]). Note that tDMRG has been employed recently for dissipative dynamics of cold atoms [21, 22].

Stroboscopic many-body dynamics. We will focus on the expansion of an interacting cloud from an initially confined state. For 2-species fermions, such an expansion has been recently observed in 2D [15] and theoretically discussed for 1D [23]. We will first briefly address the evaporation itself and then discuss qualitatively the resulting stroboscopic dynamics, with a more refined analysis presented further below. Figures 1(b)-(d) show the effect of the interaction on the unmeasured time evolution of the density profile. For increasing interaction the fermions tend to remain localized near their initial positions. For interaction strengths $|V/J| \gtrsim 3$ and the times shown here, $Jt < 16$, a more detailed analysis reveals that evaporation proceeds via the rare event of a single fermion dissociating from the edge of the cloud. The particle then moves away ballistically. This evaporation process is hindered by the formation of bound states. This is a crucial phenomenon that we will also encounter in the context of repeated measurements. For smaller interaction strengths ($|V/J| \lesssim 2$), the fermions split gradually into a larger and larger number of clusters as time increases. The parameter regimes in which the model (1) exhibits diffusive or ballistic transport was addressed using tDMRG in Ref. [24].

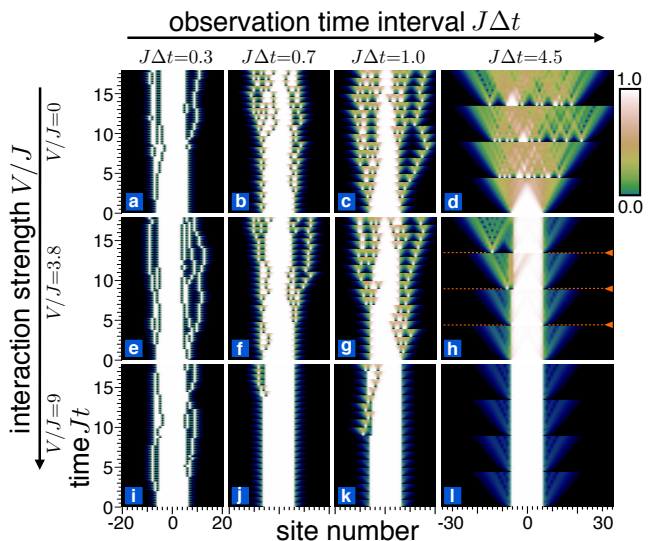


Fig. 2. (Color online) Specific realizations of the expansion of 13 fermions with site-resolved detection during the evolution. We show the full evolution of density even between observations, which collapse the many-body wave function at regular time intervals $J\Delta t$ [indicated by the dashed lines in panel (h)]. Without interaction [panels (a)-(d)], the initial decay rate of the configuration increases for larger $J\Delta t$, while for large interaction $|V/J|$ the decay rate is biggest for finite $J\Delta t$ [(g),(i)]. For small $J\Delta t$ the dynamics becomes independent of $|V/J|$, see (a),(e),(i).

The effects of stroboscopic observation are shown in Fig. 2, for typical realizations of this stochastic process. For noninteracting fermions we find the behavior expected from the single-particle case. The spread (and thus, the diffusion constant) increases with larger observation time intervals $J\Delta t$. For very small $J\Delta t$ (strong Zeno effect), the motion is diffusive with a small diffusion constant that becomes independent of $|V/J|$. In general, it is useful to discuss the *initial decay rate* of the cluster that evaporates via expansion. For the interacting case, this decay rate is largest at some finite observation time interval $J\Delta t$ [Figs. 2(g) and 2(i)], while it is reduced for large $J\Delta t$ [Figs. 2(h) and 2(l)]. Apparently, at very large $|V/J|$, the initial decay rate may have yet another local minimum for intermediate $J\Delta t$, see Fig. 2(j). We confirm this striking nonmonotonous behavior of the initial decay rate by simulating 400 realizations for each panel shown in Fig. 2 and plot the average number of fermions at the central 15 lattice sites as a function of time, in Fig. 3. For sufficiently large $|V/J|$, this number decays roughly linearly at a rate that sets the initial decay rate. We will see that these features can be mainly attributed to a bound state and the two-level dynamics between the initial state and the state with a fermion detached from the others.

Doublets and the role of interactions. The effect of interactions can be discussed already for the stroboscopic

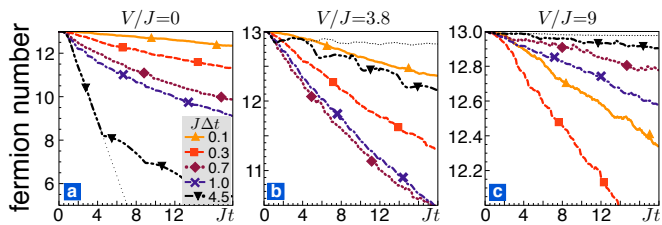


Fig. 3. (Color online) For the expansion process of Fig. 2, the average number of fermions remaining at the 15 central lattice sites is shown as function of the evolution time Jt for different observation time intervals $J\Delta t$. Thin dotted lines correspond to expansions without observation. (a) Without interactions, the initial decay rate increases monotonically with $J\Delta t$. (b) At $V/J = 3.8$, the decay rate first increases, then decreases with $J\Delta t$. (c) At $V/J = 9$, the decay rate is nonmonotonous even for intermediate $J\Delta t$; compare $J\Delta t = 0.3, 0.7, 1.0$. Note that the lines in (a)-(c) are almost identical for $J\Delta t = 0.1$.

dynamics of two fermions. We focus on the decay of a doublet, i. e., two fermions sitting at neighboring sites.

In the quantum Zeno limit, $J\Delta t \ll 1$ (or $J\Delta t \ll |2J/V|$ for large $|V|$, see below), only single hopping events occur during Δt . The probability for a fermion hopping left or right in this time interval is $2(J\Delta t)^2$. Thus, the average decay time of a doublet is $\langle Jt \rangle = 1/(2J\Delta t)$, independent of V . This result holds also for clusters of more fermions, where the leftmost and rightmost fermion dissolves with probability $(J\Delta t)^2$ during Δt [cf. Figs. 2(a), 2(e), and 2(i)].

For larger $J\Delta t$, the interaction will become important, which gives rise to a bound state (this effect also exists for clusters of more particles [25]). Considering the basis $|l, K\rangle = \frac{1}{\sqrt{N}} \sum_j \exp\{iK[j + l/2]\} c_j^\dagger c_{j+l}^\dagger |\text{vac}\rangle$ of the 2-particle sector with (positive) relative coordinate l , center-of-mass (c.m.) coordinate $j + l/2$, and total wavenumber $K = (k_1 + k_2) \bmod 2\pi$, the action of the Hamiltonian (1) is $\hat{\mathcal{H}}|l, K\rangle = |K\rangle \otimes \hat{\mathcal{H}}_K|l\rangle$. The first part describes a plane wave with wavenumber K , the second the relative motion given by

$$\hat{\mathcal{H}}_K|l\rangle = -2J_K [|l+1\rangle + (1 - \delta_{l,1})|l-1\rangle] + V\delta_{l,1}|l\rangle, \quad (2)$$

with K -dependent hopping amplitude $J_K = J \cos(K/2)$. A bound state exists if $|V| \geq |2J_K|$. It is given by $|\psi_K\rangle \propto \sum_{l=1}^{\infty} (-2J_K/V)^{l-1} |l\rangle$. We now discuss the decay of a doublet [see Fig. 4(a)] by means of the doublet survival probability $P_D(t)$, i. e., the probability of finding the doublet intact after time t . Without observations, $P_D(t) = \sum_{L'} \langle l=1, L' | e^{-i\hat{\mathcal{H}}t} | l=1, L' \rangle|^2$, where L and L' are c.m. coordinates. Thus, in the limit $t \rightarrow \infty$, we find $P_D(\infty) = \frac{1}{2\pi} \int_0^{2\pi} dK |\langle \psi_K | l=1 \rangle|^4$. Specifically for large interaction $|V/2J| \geq 1$, we have

$$P_D(\infty) = 1 - (2J/V)^2 + \frac{3}{8} (2J/V)^4. \quad (3)$$

While $P_D(\infty)$ is determined by the bound state, the evolution for times $Jt < 1$ can be approximated by the two-

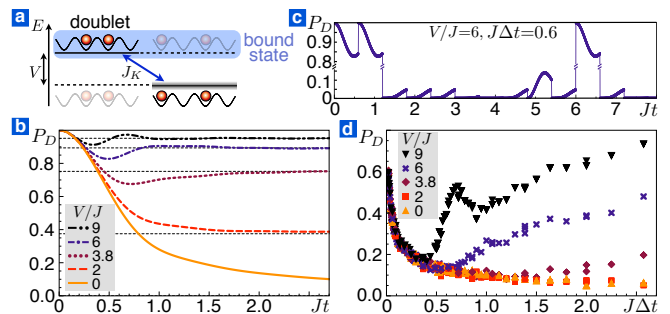


Fig. 4. (Color online) (a) Doublet decay level scheme. The doublet is separated from the continuum of unbound states by an energy gap V . (b) Probability P_D of finding the doublet intact after evolution time Jt . Dashed horizontal lines show $P_D(\infty)$ found in Eq. (3). (c) Single trajectory of P_D for a time evolution subject to observations. (d) Doublet survival probability P_D as function of the observation time interval $J\Delta t \geq 0.02$ for a fixed total evolution time $Jt = 18$. Note the non-monotonous dependence on $J\Delta t$ for finite interactions.

level dynamics between $|l=1\rangle$ and $|l=2\rangle$. This gives

$$P_D(t) = 1 - \frac{1}{\pi} \int_0^\pi dK \frac{\cos^2(K/2)}{\xi_K^2} \sin^2(2\xi_K Jt), \quad (4)$$

with $\xi_K = [(\frac{V}{4J})^2 + \cos^2(K/2)]^{1/2}$. In the strongly interacting regime we find three regions for the doublet survival probability: for times $Jt \ll \xi_{K=0}^{-1}$ the probability is independent of the interaction strength, $P_D(t) = 1 - 2(Jt)^2$; for times $\xi_{K=0}^{-1} \lesssim Jt \lesssim 1$ one expects an oscillating behavior of $P_D(t)$ given by Eq. (4) with a period approximately $\frac{2\pi}{V}$ for $|V/4J| \gg 1$; and for $Jt \gg 1$ the probability approaches $P_D(\infty)$. The full evolution of $P_D(t)$ using exact diagonalization is shown in Fig. 4(b). $P_D(t)$ is interaction-independent at times $Jt \lesssim \xi_{K=0}^{-1}/2$. Temporal oscillations in $P_D(t)$ develop for higher interaction strengths ($V/J \gtrsim 3.5$). These oscillations suggest that in the presence of stroboscopic observations, illustrated in Fig. 4(c), the survival probability will depend nonmonotonically on the observation time interval. This effect is confirmed in Fig. 4(d). In that figure, the observation time interval $J\Delta t$ is varied, while keeping the total evolution time constant, $Jt = 18$ (with a corresponding number of observations $t/\Delta t$). The stroboscopic evolution is interaction independent for small $J\Delta t$. For larger $J\Delta t$ there is a drastic recovery of P_D in the strong interacting case, which can show oscillations as a function of $J\Delta t$. This behavior agrees with the one of clusters of more fermions, see Figs. 2 and 3, and does not depend in detail on the total time Jt . Thus we have found and explained the most prominent features of the stroboscopic many-body dynamics in our discussion of the doublet.

Furthermore, the motion of whole clusters of fermions through the lattice and the exchange of fermions between clusters can be observed in the stroboscopic dynamics, as shown in Fig. 5. As expected, clusters are very stable for

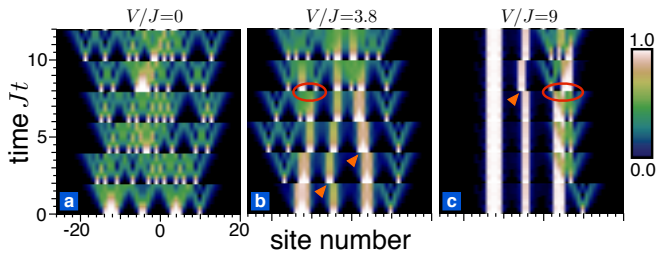


Fig. 5. (Color online) Density plot for the time evolution of an initial state with clusters of different numbers of fermions and observation time interval $J\Delta t = 2$. For large interaction strength [panels (b) and (c)], we find clusters moving as a whole (indicated by triangles). Ovals indicate processes where single fermions are exchanged between clusters or attached to a new cluster.

high interaction strengths. The hopping amplitude for a cluster of n fermions is of order $J^n/|V|^{n-1}$, decreasing strongly for larger clusters, as can be perceived in Fig. 5(c).

Expectations for other models. The previously discussed nonmonotonic decay of a cluster is not unique for our model (1), but can also be observed in the Fermi-Hubbard (FH) and Bose-Hubbard (BH) models. In the following we will consider clusters of doubly occupied sites in 1D. The dissolution of a single particle from the edge of the cluster is well described by considering the survival probability of a doublon (fermionic or bosonic double occupancy). Using a similar analysis as for the doublets, one finds qualitatively the same behavior as shown in Fig. 4(b). However, this description is not sufficient to understand the decay of clusters. It does not include the escape of paired particles, which leads to a complete decay of the cluster in the long time limit even for large onsite interaction. It also neglects tunneling of bosons between occupied sites. In the FH model the cluster is initially Pauli blocked [as in model (1)], such that the dynamics is restricted to the edges. The escape of single fermions or doublons can be well approximated by the Hubbard dimer model, see [23]. The associated probability is $\sin^2(\sqrt{V^2 + (4J)^2 t/2})/[2 + 2(J/4V)^2]$ for single fermions (at times $Jt \ll 1$) and for doublons it is $(Jt)^4$ for $Jt \ll J/V$ and $4(J^2 t/V)^2$ at $J/V \ll Jt \ll 1$. We numerically verified that this oscillating behavior of the single fermion escape leads to nonmonotonic decay of the cluster for onsite interaction strengths $V/J \geq 4$, see Fig. 6(a). The probability for an initial bosonic cluster configuration of N sites to be destroyed is for short times given by $4[1 + 3(N-1)](Jt)^2$. The first term in brackets stems from a single boson escaping from the edge, while the second and larger contribution comes from a boson tunneling between occupied sites. For larger times we studied numerically the destruction of clusters [see Fig. 6(b)] and find that the survival probability of the initial cluster configuration displays a nonmonotonic be-

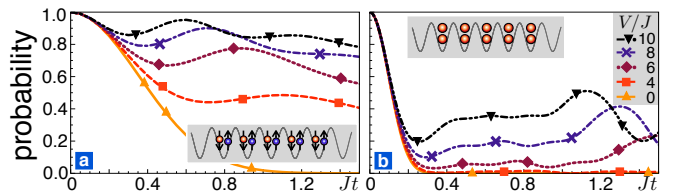


Fig. 6. (Color online) Destruction of a cluster in the 1D Fermi-Hubbard (a) and Bose-Hubbard model (b). We show the probability to detect a cluster of five doublons, see insets, in its initial state as a function of time for different onsite interaction strengths V .

havior for $V/J \geq 6$ with a pronounced local minimum at $t \approx \pi/V$ (about half the oscillation period for the dissolution of a boson and tunneling of a boson between doubly occupied sites), and the cluster is destroyed primarily via “internal” hopping processes. Both models show a strong nonmonotonic behavior of the cluster decay probability for large onsite interaction strengths. Thus, by tuning the time interval between observations in a stroboscopic measurement, one is able to enhance and suppress the decay of clusters, or even different decay channels of the cluster.

Experimental realization and outlook. The Hamiltonian (1) is related to the Heisenberg XXZ model by Wigner-Jordan transformation. The stroboscopic dynamics is identical for both models as the outcome of observations depends only on spatial density-density correlations. These Hamiltonians can be experimentally realized in optical lattices with fermionic polar molecules [26] or 2-species fermions or bosons in the insulating phase [27, 28]. For both realizations single-site detection has not yet been implemented, but experimental progress is being made toward this goal. Experimentally, the most challenging step needed to observe the interplay of many-body dynamics and measurements discussed here would be to make the observations nondestructive, whereas currently atoms are heated into higher site orbitals and atom pairs are lost due to light-induced collisions [3, 4]. Beyond the scenarios discussed here, one may also be interested in the influence of external driving or measurements that either are weak or target only specific sites.

Financial support by the DFG through NIM, SFB/TR 12, and the Emmy-Noether program is gratefully acknowledged.

-
- [1] I. Bloch, J. Dalibard, and W. Zwerger, *Rev. Mod. Phys.* **80**, 885 (2008).
 - [2] M. Lewenstein *et al.*, *Adv. Phys.* **56**, 243 (2007).
 - [3] W. S. Bakr *et al.*, *Nature* **462**, 74 (2009).

- [4] J. F. Sherson *et al.*, *Nature* **467**, 68 (2010).
- [5] C. Weitenberg *et al.*, *Nature* **471**, 319 (2011).
- [6] B. Misra and E. C. G. Sudarshan, *J. Math. Phys.* **18**, 756 (1977).
- [7] W. M. Itano *et al.*, *Phys. Rev. A* **41**, 2295 (1990).
- [8] M. C. Fischer, B. Gutiérrez-Medina, and M. G. Raizen, *Phys. Rev. Lett.* **87**, 040402 (2001).
- [9] P. Facchi and S. Pascazio, *J. Phys. A* **41**, 493001 (2008), and references therein.
- [10] N. Syassen *et al.*, *Science* **320**, 1329 (2008).
- [11] J. J. García-Ripoll *et al.*, *New J. Phys.* **11**, 013053 (2009).
- [12] A. J. Daley *et al.*, *Phys. Rev. Lett.* **102**, 040402 (2009).
- [13] R. Schützhold and G. Gnanapragasam, *Phys. Rev. A* **82**, 022120 (2010).
- [14] V. S. Shchesnovich and V. V. Konotop, *Phys. Rev. A* **81**, 053611 (2010).
- [15] U. Schneider *et al.*, arXiv:1005.3545v1.
- [16] For Supplemental Material, see Appendix.
- [17] G. Vidal, *Phys. Rev. Lett.* **93**, 040502 (2004).
- [18] A. J. Daley *et al.*, *J. Stat. Mech.* (2004) P04005.
- [19] S. R. White and A. E. Feiguin, *Phys. Rev. Lett.* **93**, 076401 (2004).
- [20] P. Schmitteckert, *Phys. Rev. B* **70**, 121302(R) (2004).
- [21] H. Pichler, A. J. Daley, and P. Zoller, *Phys. Rev. A* **82**, 063605 (2010).
- [22] P. Barmettler and C. Kollath, *Phys. Rev. A*, **84**, 041606(R) (2011).
- [23] J. Kajala, F. Massel, and P. Törmä, *Phys. Rev. Lett.* **106**, 206401 (2011).
- [24] S. Langer *et al.*, *Phys. Rev. B* **79**, 214409 (2009).
- [25] B. Sutherland, *Beautiful Models* (World Scientific, 2004).
- [26] H. P. Büchler, A. Micheli, and P. Zoller, *Nature Physics* **3**, 726 (2007).
- [27] L.-M. Duan, E. Demler, and M. D. Lukin, *Phys. Rev. Lett.* **91**, 090402 (2003).
- [28] J. J. García-Ripoll and J. I. Cirac, *New J. Phys.* **5**, 76 (2003).

SUPPLEMENTAL MATERIAL

Numerical implementation of the single-site resolved observation

An ideal single-site resolved observation of particles is a projective measurement in the basis of many-particle configurations (occupation number states in real space). However, due to the exponentially large number of states, we need a numerically efficient way to sample such outcomes. This is achieved by generating the measurement outcomes in a stepwise fashion, building on the fact that (positive) n -particle densities ρ_n factorize into conditional probabilities

$$\rho_n(s_1, \dots, s_n) = \rho_1(s_1) \cdot \prod_{i=2}^n \rho_i(s_i | s_{i-1}, \dots, s_1). \quad (5)$$

Here, $s_i \in \{1, \dots, N_s\}$ denotes the site of the i th particle and $\rho_i(s_i | s_{i-1}, \dots, s_1)$ is the conditional probability of finding the i th particle at site s_i given that there are $i - 1$ particles at the sites s_1, \dots, s_{i-1} . The procedure starts by randomly drawing the position of the first particle from a distribution given by the one-particle density. In the next step, we draw the position of the second particle, *conditioned* on the location of the first one, and continue iteratively. This way less than $n \cdot N_s$ values of joint probability densities have to be calculated, in comparison to the full number $\binom{N_s}{n}$ of fermionic many-body configurations. This approach relies on being able to calculate efficiently both the pure time evolution between observations and the i -particle densities ($1 \leq i \leq n$). In the present work, we use the time-dependent density-matrix renormalization group, which is an extremely powerful method for interacting one-dimensional systems. For the model considered in the main article, it is numerically even more efficient to draw the position of the first particle as before and then project the state onto those configurations where a particle is present at the selected site. After rescaling the resulting state, the new one-particle density is calculated. From this distribution we draw the position of the second fermion, excluding all sites already occupied by a fermion, and iterate the steps for the remaining fermions. For a discussion about local measurements on quantum many-body systems using matrix product states, see [1].

Stroboscopic dynamics of noninteracting fermions

In the noninteracting case, we can explicitly calculate the n -particle densities needed to simulate the stroboscopic dynamics. After each observation, the many-particle wave function is a Slater determinant of single-particle wave functions, and for noninteracting fermions this remains true even during the subsequent time evolution. Using Wick's theorem, the n -particle density of N fermions at time t can be written as (see also [2]):

$$\rho_n(s_1, \dots, s_n; t) = \begin{vmatrix} M_{s_1 s_1}(t) & \dots & M_{s_1 s_n}(t) \\ \dots & & \dots \\ M_{s_n s_1}(t) & \dots & M_{s_n s_n}(t) \end{vmatrix}. \quad (6)$$

Here, $M_{s_k s_l}(t) = \sum_{j=1}^N T_{s_k m_j}(t) T_{s_l m_j}^*(t)$, with the fermion propagator $T_{kl}(t) = i^{(k-l)} \mathcal{J}_{k-l}(2Jt)$, and the sum is taken over all initially occupied sites m_j . Note that the one-particle density $\rho_1(t)$ is just the sum of the densities of the individual fermions, cf. Fig.1(b) in the main article. Motion in arbitrary potentials would be captured by different propagators $T_{kl}(t)$.

[1] S. Gammelmark and K. Mølmer, Phys. Rev. A, **81**, 012120 (2010).

[2] P.-O. Löwdin, Phys. Rev. **97**, 1474 (1955).